Stern- und Planetenentstehung
Sommersemester 2020

Markus Röllig

Lecture 9: The Initial Mass Function

http://exp-astro.physik.uni-frankfurt.de/star_formation/index.php

VORLESUNG/LECTURE

Raum: Physik - 02.201a
dienstags, 12:00 - 14:00 Uhr

SPRECHSTUNDE:

Raum: GSC, 1/34, Tel.: 47433, (roellig@ph1.uni-koeln.de)
dienstags: 14:00-16:00 Uhr

Nr.	Thema	Termin
1	Observing the cold ISM	21.04.2020
2	Observing Young Stars	28.04.2020
3	Gas Flows and Turbulence Magnetic Fields and Magnetized Turbulence	05.05.2020
4	Gravitational Instability and Collapse	12.05.2020
5	Stellar Feedback	19.05.2020
6	Giant Molecular Clouds	26.05.2020
7	Star Formation Rate at Galactic Scales	02.06.2020
8	Stellar Clustering	09.06.2020
9	Initial Mass Function – Observations and Theory	16.06.2020
10	Massive Star Formation	23.06.2020
11	Protostellar disks and outflows – observations and theory	30.06.2020
12	Protostar Formation and Evolution	07.07.2020
13	Late Stage stars and disks – planet formation	14.07.2020

9 Initial Mass Function – Observations and Theory

IMF: how does a cluster break up into individual stars

9.1 Observations

- direct star counts
- integrated light from more distant regions

9.1.1 Resolved Stellar Populations

9.1.1.1 Field Stars

1st attempt: Salpeter (1955), stars in solar neighborhood

Steps to measure IMF of the field stars in some volume or angular region around the sun?

CONSTRUCT THE LUMINOSITY FUNCTION

- absolute luminosities require distances (also to determine which stars fall into a volume limited sample)
- most accurate: parallax measurements
  - IMF needs to be sampled down to low masses
  - low mass stars are very dim
  - parallax of dim stars hard to determine

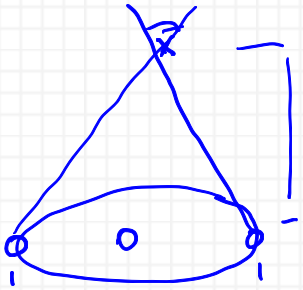

E.g.: $M \sim 0.1\ M_{\odot}$ => V band magnitudes $M_V \sim 14$, parallax catalogs at such magnitudes usually available out to 5-10 pc, i.e. 200-300 stars. (OUTDATED)

- less accurate but much larger samples
  color-magnitude diagrams (CMD) calibrated with solar neighborhood stars
  - stars with unknown distance are assigned an absolute magnitude based on their color and the CMD.

$$m - M = 5 \log\left(\frac{d}{1pc}\right) - 5$$

distance modulus $m - M$

m: apparent mag.

M: abs. mag.

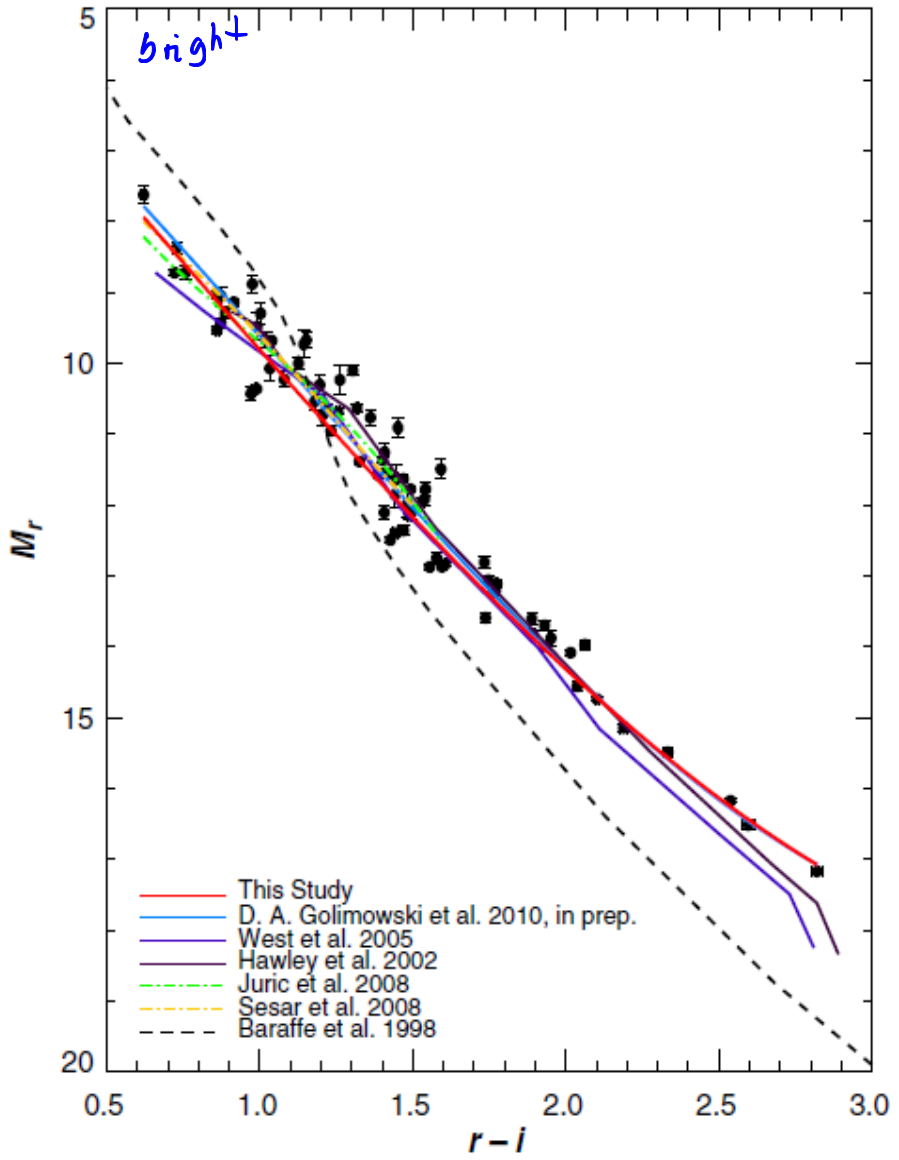

Figure 7. M_r vs. $r-i$ CMD. The parallax stars from the nearby star sample are shown as filled circles, and the best-fit line from Table 4 is the solid red line. Other existing parallax relations are plotted for comparison: West et al. (2005, purple dash-dotted line), Jurić et al. (2008, their "bright" relation; green dash-dotted line), Sesar et al. (2008, yellow dash-dotted line), and D. A. Golimowski et al. (2010, in preparation, solid blue line). The original West et al. (2005) relations have been transformed using the data from their Table 1. In addition, the 5 Gyr isochrone from the Baraffe et al. (1998) models appears as the dashed line.

Abbildung 1 Bochanksi et al. 2010, Copyright of the AAS

- spectral parallax method (analog to CMD, but with spectral-type – magnitude diagrams STMD)

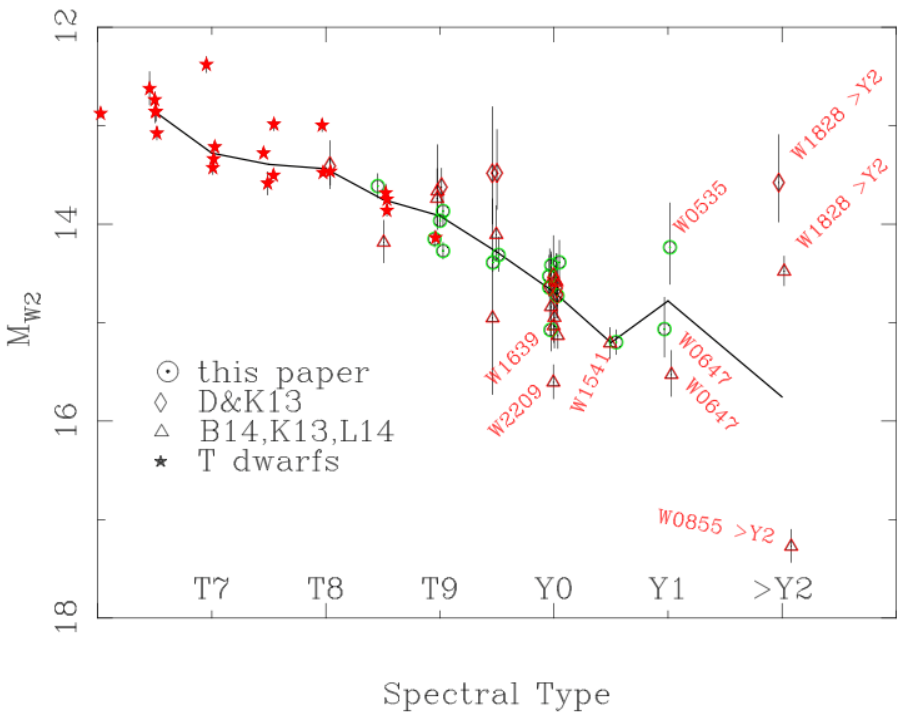

Abbildung 2 Tinney et al. 2014, The Luminosities of the Coldest Brown Dwarfs, Copyright of the AAS

BIAS CORRECTION

- Metallicity Bias
  - metallicity gradient in Galaxy, remote stars will have lower average metallicity
  - lower metallicity stars: higher T_{eff} and earlier spectral types
  - sub-solar stars will be assigned too high abs. luminosities based on color (-> too large distances)
  - **correction with known metallicity gradient**

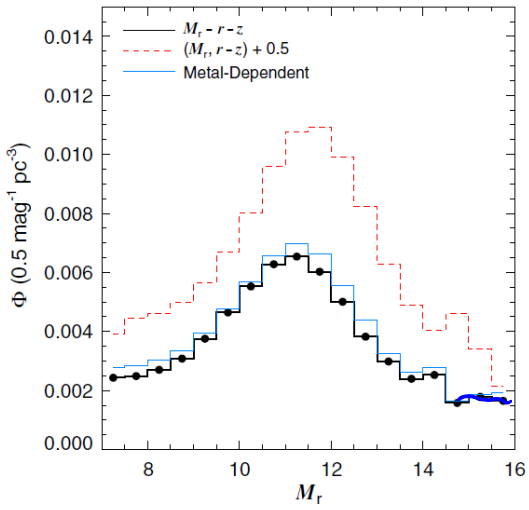

Figure 16. Differences in the LF induced by metallicity gradients, along with the raw LF (black line). The red histogram corresponds to the extreme limit, where all stars are metal-poor ([Fe/H] ~ -0.65). The blue histogram shows the effect of the metallicity gradient from Equation (9).

Figure 1 Bochanksi et al. 2010, Copyright of the AAS

- Extinction bias
  - dust extinction reddens starlight
  - more distant stars are artificially red -> low magnitudes
  - abs. magnitudes and distances are underestimated
  - **correction with known extinction curve (and known? amount of extinction per distance)**

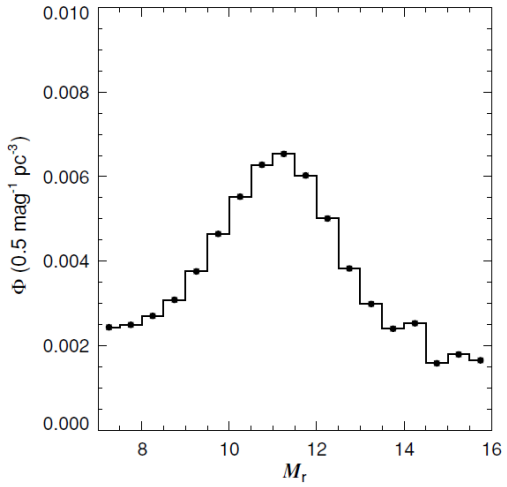

Figure 15. Raw r-band LF for the stellar sample, using the $(M_r, r-z)$ CMR. Note the smooth behavior, with a peak near $M_r \sim 11$, corresponding to a spectral type of ∼M4. The error bars (many of which are smaller than the points) are the formal uncertainties from fitting the local densities in each 0.5 mag absolute magnitude slice in stellar density.

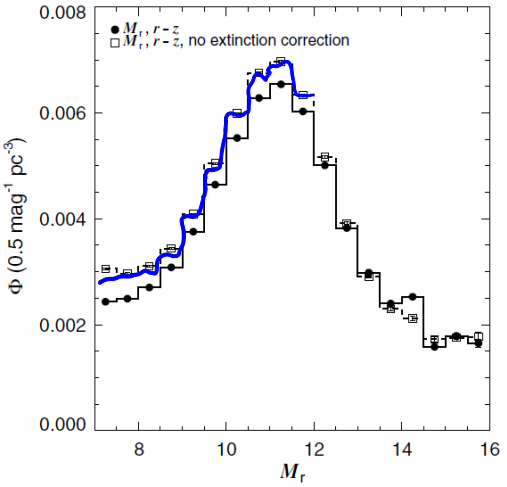

Figure 17. Systematic effect of extinction on the raw LF. When no extinction correction is applied (open squares), distant stars act to inflate the local densities of the brightest stars, compared to the fiducial case (filled circles). At fainter luminosities, this effect becomes less important.

Abbildung 3 Bochanski et al. 2010, Luminosity function (LF) for Milky Way stars before (left) and after (right) extinction correction. Copyright of the AAS

- Malmquist bias (Malmquist 1922)
  - scatter of magnitudes of stars at fixed color (up or down)
  - effect on stars at distance or magnitude limit of survey
  - **Correction if scatter distribution and sample selection is known**

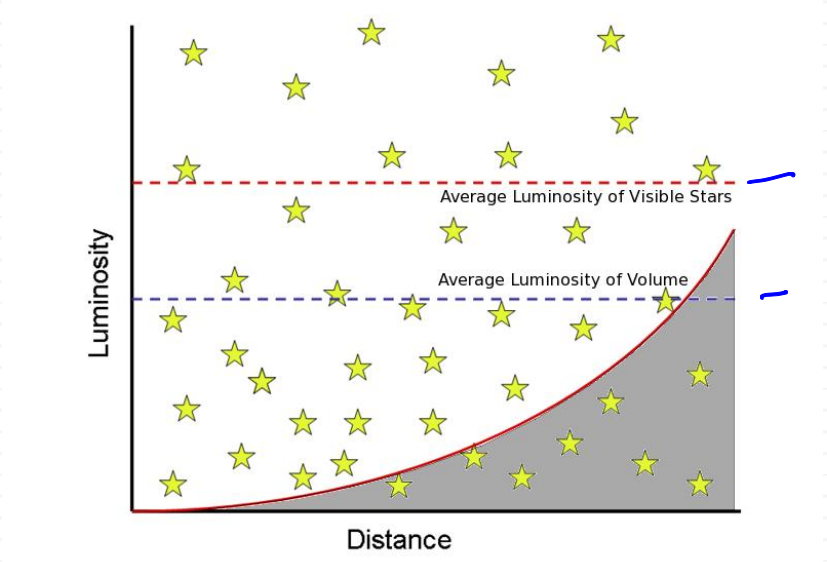

Abbildung 4 Malmquist bias. Inverse square law makes all stars below red curve invisible in the sample. As a consequence, from the more distant stars, only the brighter ones are visible shifting the apparent average luminosities within a volume to higher values. Any inherent scatter of stellar luminosities close to the limit will remove these stars from the sample if they scatter below the red curve, shifting the average line to higher values. This effect is asymmetric, because if they scatter to higher luminosities the effect on the average curve is much smaller because they stay in the sample.

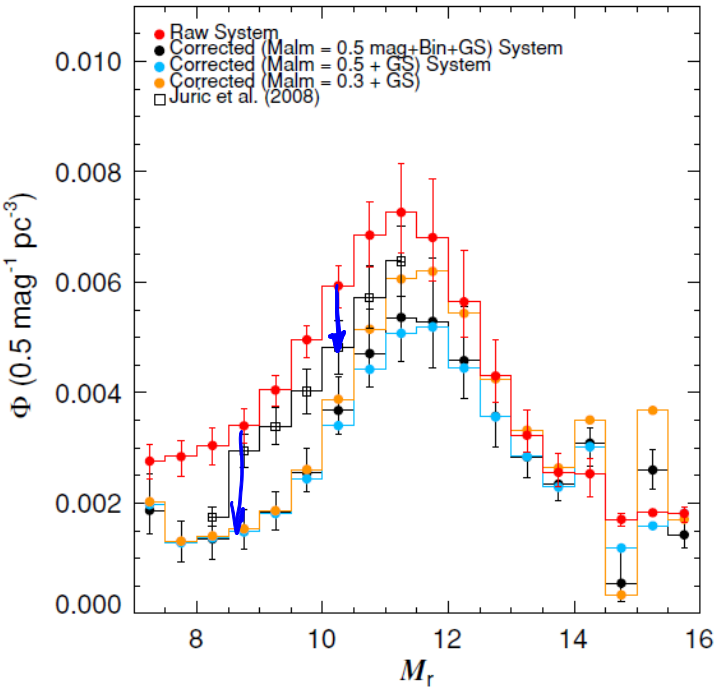

Figure 19. Effects of Malmquist bias (orange and blue filled circles), unresolved binarity (black), and GS on the survey. The mean observed LF is larger than the corrected LF at most bins. The largest effects are seen for the brightest stars, which are subject to the largest shifts due to a change in the thin disk scale height. The difference between the orange and blue LFs demonstrates the sensitivity of the Malmquist correction to the assumed scatter in the main sequence. The binary correction becomes relatively more important at fainter absolute magnitudes. The LF from Jurić et al. (2008, open squares) is shown for comparison to our raw system LF. They did not probe faint absolute magnitudes, employed a different CMR, and did not correct their densities for Malmquist bias, which accounts for the offsets between their LF and ours.

Figure 2 Bochanski et al. 2010 Copyright of the AAS

- Binarity bias
  - many stars are members of a binary system
  - remote binaries unresolved (and mistake for a single star)
    - binary of unequal mass $q = \frac{M_2}{M_1} \lesssim 0.3$ $L \sim M^{3.5}$
      - color and magnitude dominated by massive companion
      - low mass companion invisible (missed)
    - equal mass binaries $q \sim 1$
      - color stay the same
      - CMD assigns luminosity of single star (true luminosity twice that high)
      - underestimate the distance
      - artificially scatter the system into the survey (if volume limited) or out of survey (if luminosity-limited)
  - correction if binarity fraction of mass ratio is known

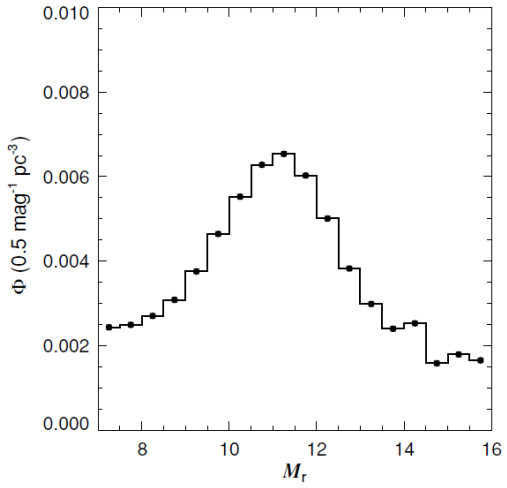

Figure 15. Raw r-band LF for the stellar sample, using the $(M_r, r-z)$ CMR. Note the smooth behavior, with a peak near $M_r \sim 11$, corresponding to a spectral type of ~M4. The error bars (many of which are smaller than the points) are the formal uncertainties from fitting the local densities in each 0.5 mag absolute magnitude slice in stellar density.

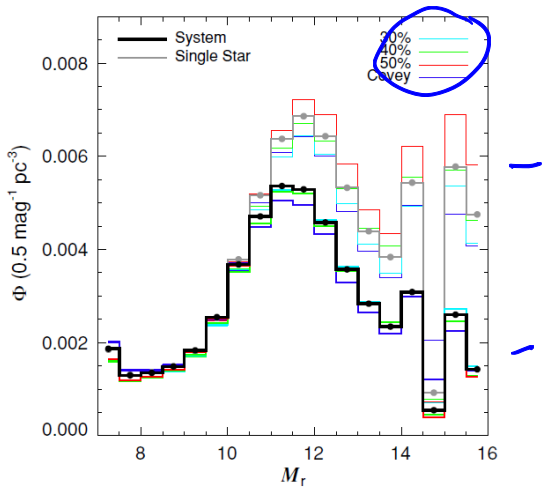

Figure 20. System and single-star M_r LFs for our four different binary prescriptions. The spread between prescriptions in each bin is used to calculate the final uncertainty in the system and single-star LFs.

Abbildung 5 Bochanski et al. 2010, Luminosity function (LF) for Milky Way stars before (left) and after (right) binary bias correction (assuming various binarity fractions). Copyright to AAS

MASS-MAGNITUDE RELATION

- Convert LF into a mass function
  - requires a mass-magnitude relation (MMR)

- theoretical modelling, empirical, or both

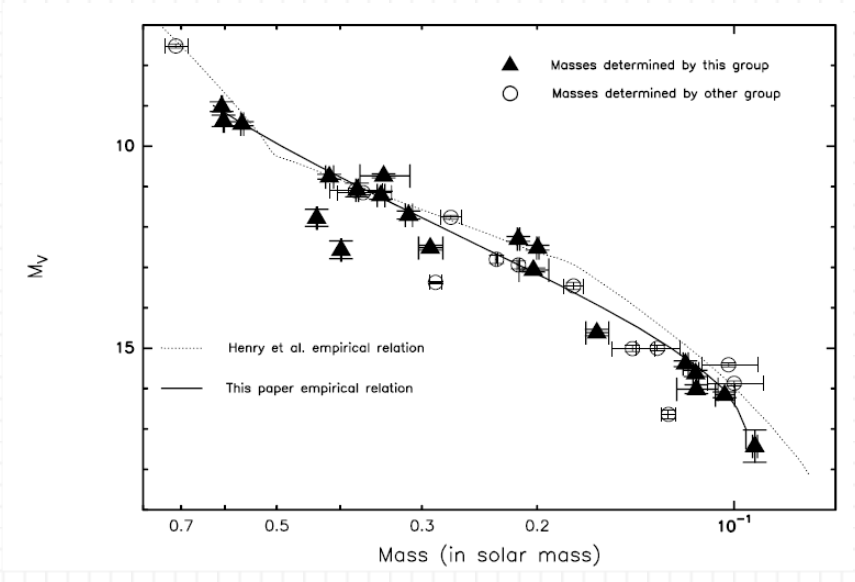

Abbildung 6 Delfosse at al. 2000, Copyright ESO 2000

Result -> IMF for stars up to $\sim 0.7\ M_\odot$

AGE CORRECTIONS

- higher mass stars evolve off the main sequence on time scales comparable to the mean stellar age in the solar neighborhood
- we measure a present-day mass function (PDMF)

If we know the SF history $\dot{M}_*(t)$ and the initial, mass-dependent main-sequence stellar lifetime $t_{MS}(M)$, then the total number of stars formed in the full lifetime of the Galaxy is:

$$\frac{dN_{form}}{dM} = \frac{dN}{dM}\int_{-\infty}^{0} \dot{M}_*(t)dt$$

$t = 0$ is today, and dN/dM is the IMF.

The number of stars still on the main sequence is:

$$\frac{dN_{MS}}{dM} = \frac{dN}{dM}\int_{-t_{MS}(M)}^{0} \dot{M}_*(t)dt$$

dN_{MS}/dM is measured. This allows to correct for the IMF by scaling the number of observed stars by the fraction of stars in that mass bin that are still alive today

$$\frac{dN}{dM} \propto \frac{dN_{MS}}{dM} \frac{\int_{-\infty}^{0} \dot{M}_*(t)dt}{\int_{-t_{MS}(M)}^{0} \dot{M}_*(t)dt}$$

Limited to masses below a few solar masses.

9.1.1.2 Young Clusters

More massive stars need different techniques – survey of young clusters.

General approach is the same as for field stars, with some advantages.

- population is young enough for even the most massive stars to remain on the MS (PDMF=IMF)
- population uniform in metallicity -> no bias
- population about the same distance -> no extinction or Malmquist bias.
    - distance is better known from radio interferometry
- Low-mass stars and brown dwarfs are much more luminous if still young

Disadvantages

- bad statistics, closest cluster where stars can be resolved: Orion Nebula Cluster (D=415pc, only 10^3-10^4 stars, compared to ~10^6 stars in largest field star survey, most massive star on $M = 38\mathrm{M}_\odot$)
- MMR is much more complicated because metallicity changes over lifetime
- youngest cluster still have significant dust content
- mass segregation (most massive stars cluster in the center, low mass stars in the outskirts). Difficult to measure the IMF over the whole cluster. Extinction not uniform.
- Dynamical effects problematic: runaway stars (O and B stars with v~50 km/s, ejected from cluster), tidal stripping will preferentially remove outskirt stars from cluster (i.e. low-mass stars)

- Binary fraction for young cluster much less well known than for field stars.

9.1.1.3 Globular Clusters

- Globular clusters are old, lack massive stars
- study IMF in conditions very different from young clusters
- template for studying unresolved SF
- dynamical effects much worse because of long lifetime
    - low mass stars are systematically lost (two-body evaporation)

9.1.1.4 General Results

- IMF appears to be fairly universal
- Exception: Nuclear Cluster of the MW with a flatter IMF (~1.7 compared to 2.35 Lu et al. 2013)

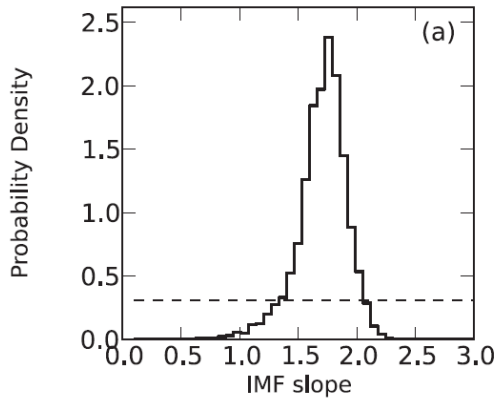

Figure 3 Lu et al. 2013, copyright to AAS

Update:

The Gaia mission has by now has (parallax, position, eigen velocity) 1.3 billion stars measured! Luminosities are available for 77 million stars.

The survey represented by Gaia DR2 is essentially complete between G=12 and G=17 mag.

At G<7 mag, however, there are still many sources missing from the catalogue, primarily due to the difficulties of treating saturated CCD images (with no stars brighter than G=1.7 mag appearing in GaiaDR2).

Fainter than G=17 mag, the completeness is affected by a combination of data processing limitations in crowded fields and the filtering applied before publication.

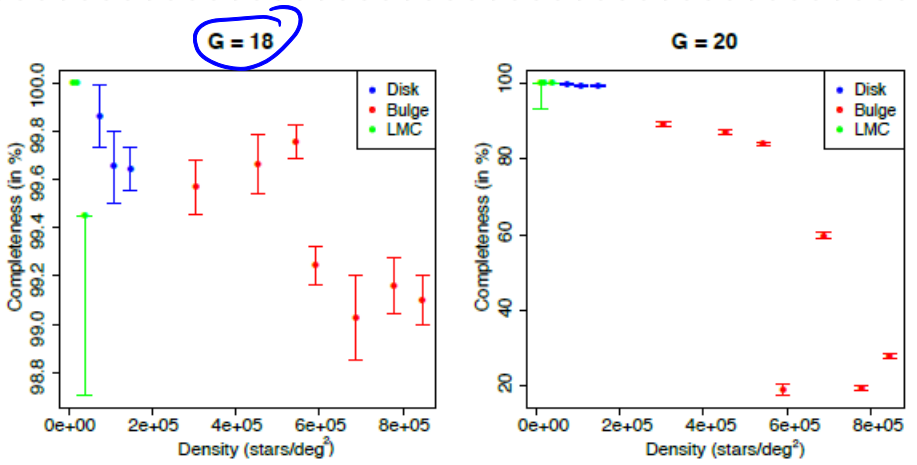

Fig. 5. *Gaia* DR2 completeness vs. some OGLE fields at $G = 18$ and $G = 20$ as a function of the measured density at $G = 20$. The scale of the two plots is very different.

Figure 4 Credits: Arenou et al. 2018 A&A 616, A17 (2018)

Based on Gaia DR2 data Sollima (2019) derived the IMF for sample of more than 120 000 stars in the solar neighborhood, with parallaxes, magnitudes and colors from the DR2:

- The shape of the initial mass function is well represented by a segmented power law with two breaks at characteristic masses.
- It has a maximum at $M \sim 0.15$ $M_\odot$ with
  - significant flattening (possibly a depletion) at lower masses and
  - a slope of $\alpha = -1.34 \pm 0.07$ in the range $0.25 < M/M_\odot < 1$.
- Above 1 $M_\odot$, the initial mass function shows an abrupt decline with a slope ranging from $\alpha = -2.68 \pm 0.09$ to $\alpha = -2.41 \pm 0.11$, depending on the adopted resolution of the star formation history.

A slope of -2.7 is significantly steeper than what has been proposed (e.g. Kroupa, Salpeter, Chabrier) before high resolution data from Hipparcos (2010) & Gaia (2018) became available.

9.1.2 Unresolved Stellar Populations

Resolved studies: only Milky Way (and Magellanic Clouds for $M > 1M_\odot$)

9.1.2.1 Stellar Population Synthesis Methods

- start with proposed IMF

- predict stellar light from stellar population with mass M_* ($L_V(M,t)$: predicted specific luminosity of star with mass M and age t)

$$L_V = M_* \int_0^\infty \frac{dN}{dM} L_V(M,t) dM$$

- given a specific star formation history on must further integrate over it:

$$L_V = \int_0^\infty \dot{M}_* \int_0^\infty \frac{dN}{dM} L_V(M,t) dM\, dt$$

- comparison of predicted spectrum with observed one
- select particular photometric filters to be sensitive to particular regions of the IMF
  - $H\alpha$ emission versus emission in other bands: diagnostics of ratio of very massive stars per unit total mass, i.e. shape of the IMF at the upper mass end
  - lower mass IMF: Na I doublet and the Wing-Ford molecular FeH band. Both absorption features only produced in M type stars but not in M giants! -> only red dwarfs!
    Strength of these two features measures the ratio of M dwarfs to K dwarfs ($\sim 0.1 - 0.3 M_\odot$ stars to $\sim 0.3 - 0.5 M_\odot$ stars)

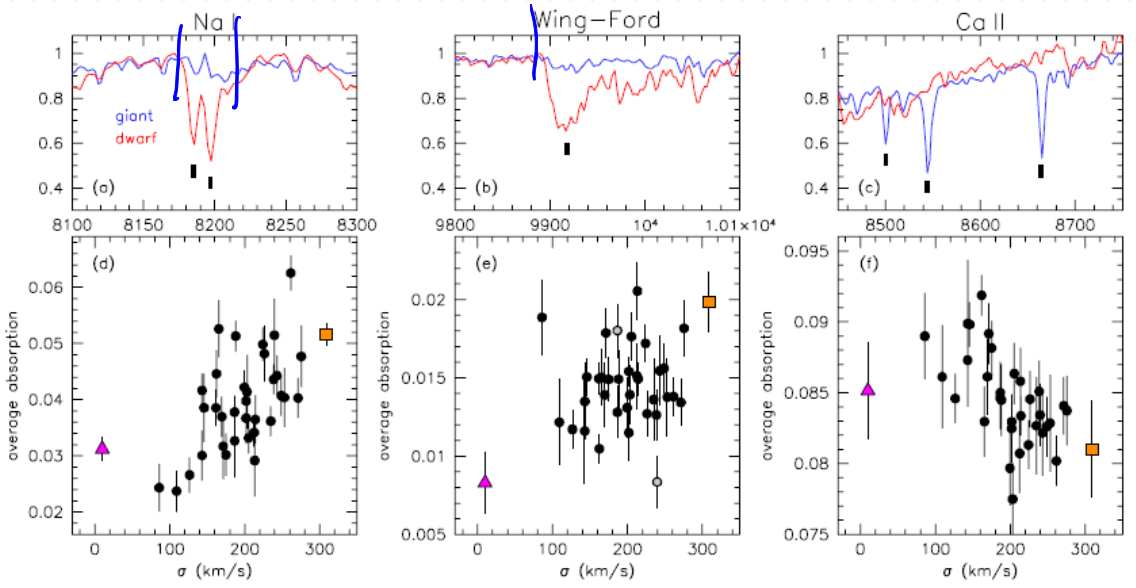

Figure 10. (a–c) The Na I doublet, the Wing–Ford band, and the Ca II triplet in the M6 dwarf Gliese 406 (red) and the M4 giant HD 4408 (blue). For a larger dwarf-to-giant ratio Na I and Wing–Ford are expected to be stronger and Ca II is expected to be weaker. (d–f) The strength of these features in integrated light, as a function of velocity dispersion. Black dots are individual SAURON galaxies. The purple triangle represents metal-rich globular clusters in M31 (van Dokkum & Conroy 2011), and the orange square is measured from the average spectrum of high-dispersion elliptical galaxies in the Virgo cluster (van Dokkum & Conroy 2010). Na I and Ca II show strong and opposing trends, consistent with more bottom-heavy IMFs for galaxies with higher dispersions. The relation between the Wing–Ford band and σ is only significant when the globular clusters and the massive Virgo galaxies are included.

Figure 5 van Dokkum & Conroy 2012, copyright to AAS

- van Dokkrum & Conroy find features that are not consistent with galactic field IMFs. Instead they found an IMF that continues to rise down to $M \sim 0.1 M_{\odot}$ (rather than having a turnover) -> highly debated.

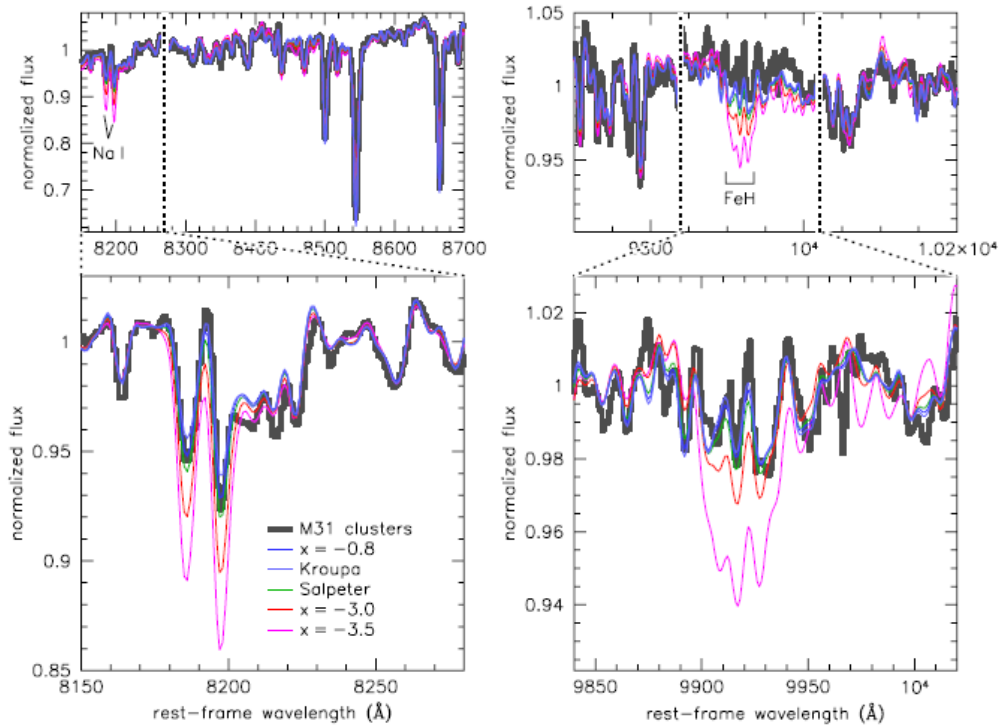

Figure 3. Averaged Keck spectra of the M31 globular clusters B143, B147, B163, and B193 (thick gray lines). The left panels show the region near the Na I doublet and the right panels show the FeH Wing–Ford band region. The bottom panels zoom in on the IMF-sensitive features. Colored lines show predictions from stellar population synthesis models with different IMFs. Models with "normal" IMFs match the data very well over the entire wavelength range. Dwarf-rich IMFs with steep slopes ($x \sim -3$)—which provide good fits to massive elliptical galaxies—do not fit the observed weak Na I doublet and Wing–Ford band of the globular clusters.

Figure 6van Dokkum & Conroy 2011, copyright to AAS, average spectra of the Virgo and Coma cluster ellipticals and model predictions.

9.1.2.2 Mass to Light Ratio Methods

- measure mass independent from starlight
  - gravitational lensing
  - dynamical modelling of the system
- divide mass map by light map to form mass-light ratio
- dark matter?

9.1.3 Binaries

9.1.3.1 Finding Binaries

1767 (!) John Mitchel performed a statistical analysis of the star distribution on the sky and concluded that there are much too many close pairs than would be expected from random placement! (Poisson distribution only described on 1838!)

- Spectroscopic binaries: spectral lines show periodic radial velocity variations -> limited to close binaries because of long periods
- Eclipsing binaries: periodic light curve variations (occultation probabilities higher for very close binaries and also their orbit times are shorter)
- Visual binaries: stars are far enough apart to resolve them

9.1.3.2 Binary Properties

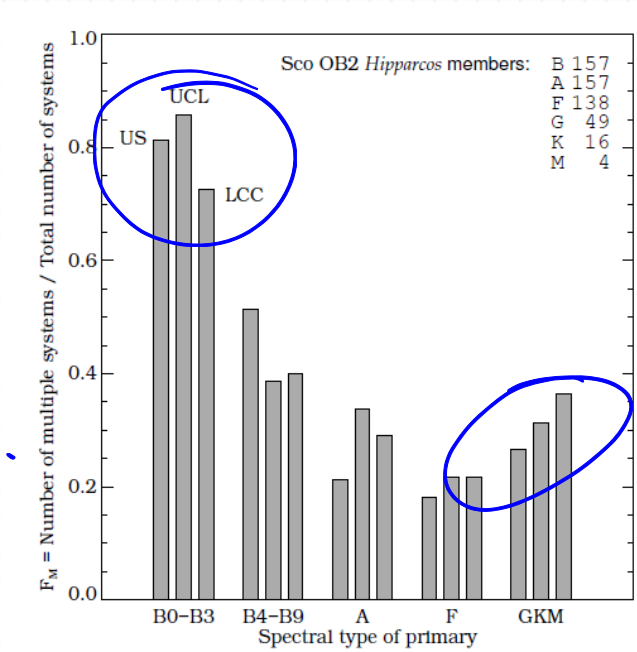

Figure 7 Kouwenhoven, M.B.N. 2006, PhD

- Binary fraction is a strong function of mass
- extremely broad period separation (distance) distribution
- close companions are much more likely to have comparable masses to the primary than if randomly sampled from IMF.

Long-period companions are consistent with randomly drawn from IMF.

9.2 THEORY

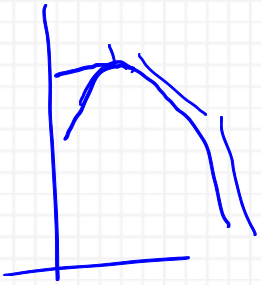

Things we would like to explain:

- slope of the power-law at high masses
- location of the peak mass
- little to zero variation with galactic environments
- origins of the distribution in binary properties

9.2.1 The Power-law Tail

$$\frac{dN}{dm} \propto m^{-\Gamma} \quad \text{with } \Gamma \approx 2.3 \quad (Salpter's\ value)$$

9.2.1.1 Competitive Accretion

A number of seed stars is formed and then begins to accrete mass at a rate that is a function of their mass.

Assume

$$\frac{dm}{dt} \propto m^{\eta}$$

We start with mass m_0, accretion rate $\dot{m}_0$ at a time t_0. Solving the ODE gives:

$$m(t) = m_0 \begin{cases} [1-(\eta-1)\tau]^{1/(1-\eta)}, & \eta \neq 1 \\ \exp(\tau), & \eta = 1 \end{cases}$$

$\tau = t/(m_0/\dot{m}_0)$ time measured in units of the initial mass-doubling time.

$\eta = 1$ gives the usual exponential growth, $\eta > 1$ grows even faster (to infinite in finite time).

Example: population of stars with m_0, but all with slightly different values of τ at which they stop growing. What will the mass distribution of the resulting population be?

If $dN/d\tau$ is the distribution of stopping times, then

$$\frac{dN}{dm} \propto \frac{dN/d\tau}{dm/d\tau} = m(\tau)^{-\eta}\frac{dN}{d\tau}$$

➔ power-law distribution in mass with index $-\eta$ going from $m(\tau_{min})$ to $m(\tau_{max})$

➔ index will depend on index of the accretion law η. What is η?

point mass accreting from uniform, infinite medium: $\dot{m} \propto m^2$ (Hoyle, Bondi) close to the actual slope of -2.3.

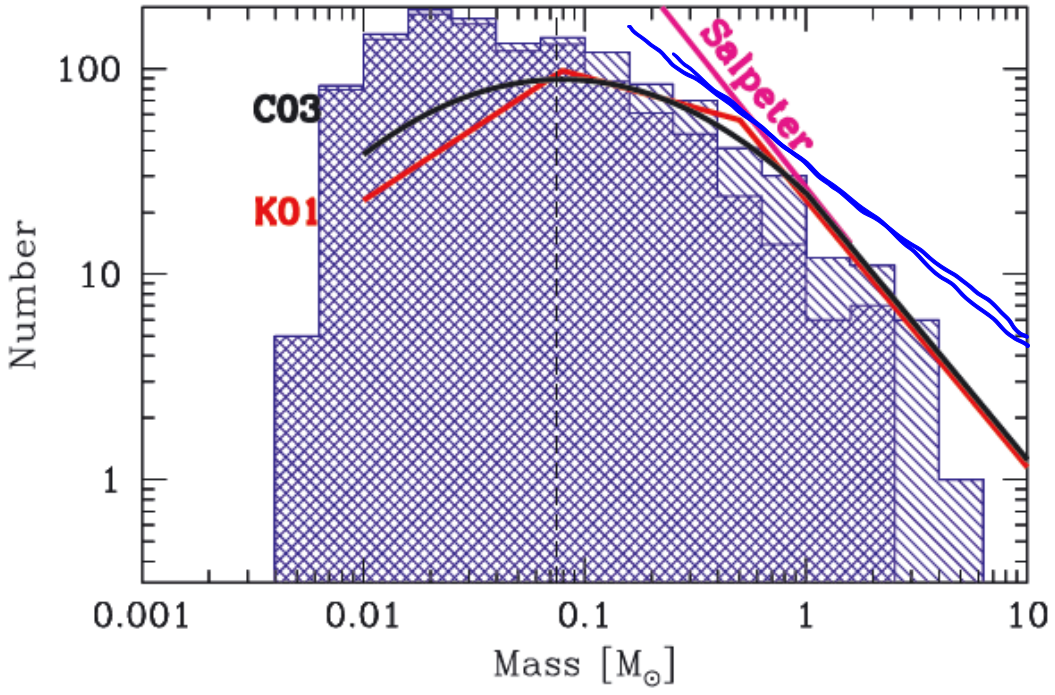

Figure 3. Histograms giving the IMF of the 1254 stars and brown dwarfs that had been produced by the end of the main calculation. The single-hashed region gives all objects, while the double-hashed region gives those objects that have stopped accreting. Parametrizations of the observed IMF by Salpeter (1955), Kroupa (2001) and Chabrier (2003) are given by the magenta line, red broken power law and black curve, respectively. The numerical IMF broadly follows the form of the observed IMF, with a Salpeter-like slope above $\sim 0.5\,M_\odot$ and a turnover at low masses. However, it clearly overproduces brown dwarfs by a factor of ≈ 4.

Fig.: Bate, M. R. 2009a, Mon. Not. Roy. Astron. Soc., 392, 590, 0811.0163

Problems:

- depends on choice of initial conditions (e.g. $\alpha_{vir} \sim 1$, no initial density structure)

- works only without feedback to drive turbulence or eject gas.
- Competitive accretion requires a 'global' collapse where all the stars fall together into a region where they can compete
- IMF peak is not reproduced

9.2.1.2 Turbulent fragmentation

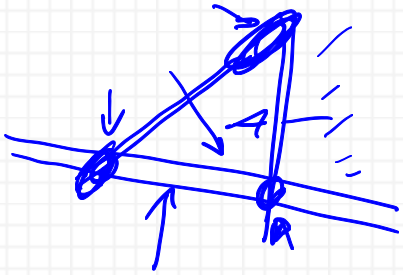

Power-law slope a result of turbulence physics.

Initially Padoan et al. 1997

Assumption:

- Shocks repeatedly passing through an isothermal medium produces a broad range of density distributions
- stars form wherever a local region happens to become self-gravitating

Suppose a density field smooth on a scale ℓ. The mass of an object of density ρ then is:

$$m \sim \rho \ell^3$$

Total mass of all objects with density between ρ and $\rho + d\rho$ is

$$dM_{tot} \sim \rho \ell^3 p(\rho) d\rho$$

$p(\rho)$: density PDF

Total number of objects in the mass range $[m, m + dm]$ on size scale ℓ:

$$\frac{dN_\ell}{dm} = \frac{dM_{tot}}{m} \sim \ell^{-3} \int p(\rho) d\rho$$

To filter out the grav. bound objects: critical density

$$\frac{Gm^2}{\ell} \sim m\sigma(\ell)^2 \implies \rho_{crit} \sim \frac{\sigma(\ell)^2}{G\ell^2}$$

$\sigma(\ell) = c_s \left(\frac{\ell}{\ell_s}\right)^{1/2}$: linewidth-size relation

Thus: $\rho_{crit} \sim \frac{c_s^2}{G \ell_s \ell}$ (lower limit of integral)

Next steps: $\frac{dN}{dm} \propto \int \frac{dN_\ell}{dm} d\ell$ to get total number of objects

Assume form of $\mathcal{p}(\rho)$

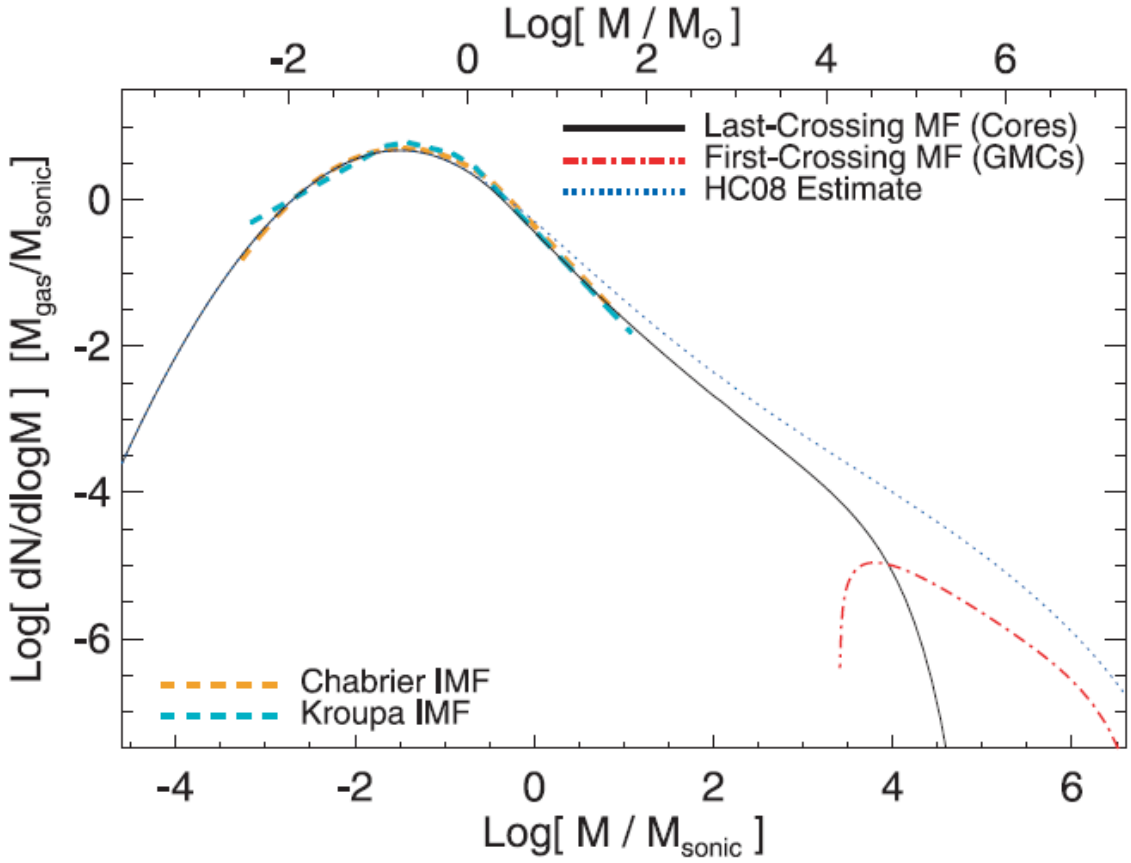

Abbildung 7 The IMF predicted by an analytical model of turbulent fragmentation by Hopkins 2012. (Philip F. Hopkins

Monthly Notices of the Royal Astronomical Society, Volume 423, Issue 3, July 2012, Pages 2037–2044, https://doi.org/10.1111/j.1365-2966.2012.20731.x)

Result (IMF) depends only on c_s and ℓ_s (sonic length)

At mass> sonic mass ($M_s \approx c_s^2 \ell_s / G$) the result gives approx. the right power-law index.

Problems:

- choice of PDF rigorous
- dependence on ℓ_s problematic (is not constant)
- does not answer why gravitationally bound regions don't sub-fragment
- IMF peak not explained

9.2.2 The peak of the IMF

9.2.2.1 Basic theory

- Power-law is scale-free
- peak has a definite mass scale
  - set by the physical process!
- isothermal model cannot explain the peak!

Qualitative argument:

The system we described contains four energies: thermal energy, bulk kinetic energy, magnetic energy, gravitational potential.

➔ 3 dimensionless ratios determine the behavior of the system

$$\mathcal{M} = \frac{\sigma}{c_s} \qquad \beta = \frac{8\pi\rho c_s^2}{B^2} \qquad n_J = \frac{\rho L^3}{c_s^3/\sqrt{G^3\rho}}$$

E_{kin}/E_{th} E_{th}/E_{mag} E_{th}/E_{grav}

Jeans number

Scaling of these ratios with density ρ, velocity dispersion σ, magnetic field strength B, and length scale L:

$$\mathcal{M} \propto \sigma \qquad \beta \propto \rho B^{-2} \qquad n_J \propto \rho^{\frac{3}{2}} L\text{^}3$$

- Assume scaling: $\rho \to x\rho, L \to x^{-1/2}L, B \to x^{1/2}B$
- Then all ratios stay the same!

- Two systems (one with: ρ, L, B, and one with: $x\rho, x^{-1/2}L, x^{1/2}B$) behave the same!
- If the first system fragments and forms a star, the second will too
- The masses of those stars are different though!
  - 1. star $M \propto \rho L^3$
  - 2. star $M \propto (x\rho)\left(x^{-\frac{1}{2}}L\right)^3 = x^{-\frac{1}{2}}\rho L^3$

Isothermal gas is scale-free!

If we have a model involving only isothermal gas with turbulence, magnetic fields, gravity, and this model creates stars of a given mass M, then we can rescale the system to obtain an arbitrarily different mass.

To explain the IMF peak we need to involve some additional physics.

9.2.2.2 The IMF from Galactic Properties

Hypothesis: The IMF is set at the outer scale of the turbulence, where the MCs join the atomic ISM. Something in this outer scale picks out the characteristic mass of stars at the IMF peak.

Simplest: IMF peak is set by the Jeans mass at the mean density of the cloud:

$$M_{peak} \propto \frac{c_s^3}{\sqrt{G^3\bar{\rho}}}$$

Problems:

- MCs don't have the same density (temperature is about equal)
- varying the density leads to a factor ~ 3 difference in M_{peak} between 10^4 and 10^6 $M_\odot$ clouds.
- cancelling this with higher temperature (because of higher density) seems to be very coincidental.

Less simple: IMF peak is set by the sound speed and the normalization of the linewidth-size relation.

$$M_{peak} \propto \frac{c_s^2 \ell_s}{G}$$

Assume a cloud of mass M and radius R

$$\alpha_{vir} \sim \frac{\sigma^2 R}{GM} \Rightarrow \sigma \sim \sqrt{\alpha_{vir} \frac{GM}{R}}$$

This is the velocity dispersion at the outer scale of the cloud. The Mach number on this scale is:

$$\mathcal{M} = \frac{\sigma}{c_s} \sim \sqrt{\alpha_{vir} \frac{GM}{R c_s^2}}$$

The sonic length scale is the length scale where $\mathcal{M} \sim 1$ (σ scales with $\ell^{1/2}$).

$$\ell_s \sim \frac{R}{\mathcal{M}^2} \sim \frac{c_s^2}{\alpha_{vir} G \Sigma}$$

$$M_{peak} \sim \frac{c_s^4}{\alpha_{vir} G^2 \Sigma}$$

Note that:

$$\frac{M_J}{\mathcal{M}} \sim \frac{c_s^3}{\sqrt{G^3 \bar{\rho}}} \sqrt{\frac{R c_s^2}{\alpha_{vir} GM}} \sim \frac{c_s^4}{\alpha_{vir} G^2 \Sigma} \sim M_{peak}$$

- naturally explains why MCs in the MW make stars at the same mass
- regions with much higher Σ produce much different M_{peak}
- cancelling with higher T ??

9.2.2.3 Non-Isothermal Fragmentation

Relax the isothermal assumption on small scales.

FIXED EXQUATION OF STATE

- low n, main heating by CR and FUV, cooling by lines (CO, CII)
- heating per nucleus constant, cooling increases with density -> temperature decreases with increasing n

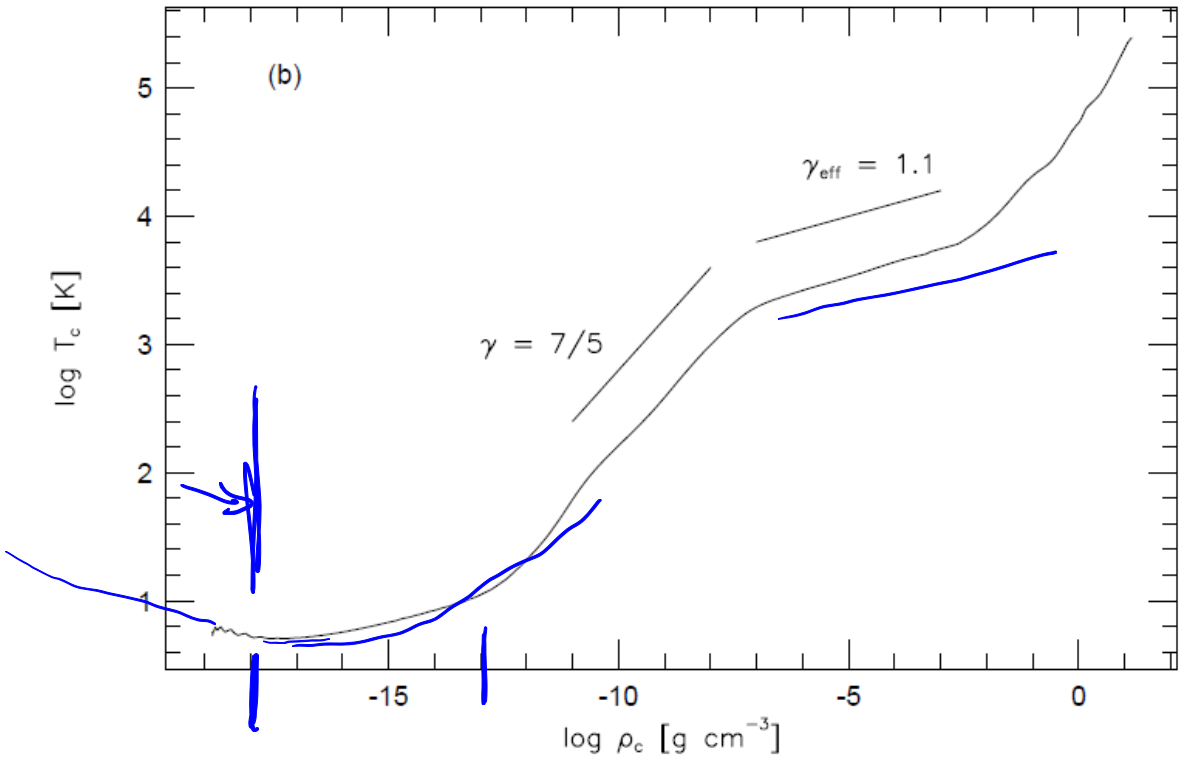

FIG. 2.—Thermal evolution at the center of the cloud core is depicted for the initially homogeneous model. The upper panel shows the energy exchange rate between gas and dust (Λ_{gd}), the radiative heating rate ($\kappa_E cE$), the radiative cooling rate ($4\pi\kappa_P B$), and the compressional heating rate of Γ_g) as functions of the central density. For $\rho_c \gtrsim 10^{-12}$ g cm^{-3} the radiative heating and cooling rates are merged. The lower panel shows the central temperature as a function of the central density.

Abbildung 8 Masunaga & Inutsuka, 2000, copyright to AAS

- If $n > n_{crit}(\mathrm{CO})$ shielding becomes important -> T decreases further
- $n > 10^5 - 10^6$ cm^{-3} $\approx 10^{-18}$g cm^{-3} lines become optically thick and cooling mainly by dust (fixed rate)
  - heating by gas collapse (compression)
  - increasing collapse speed ($t_{ff} \propto 1/n$) -> heating rate increases with n -> temperature grows

- $n > 10^{-13}\mathrm{g\,cm^{-3}}$ gas becomes optically thick to dust thermal emission -> adiabatic compression

For filaments, particularly important.

Filaments can collapse only if $T \propto \rho^{x<0}$

Collapse stops if $T \propto \rho^{x>0}$

Filaments will collapse until $n \sim 10^{-18}\mathrm{g\,cm^{-3}}$ and then break up into spheres to collapse further (Larson 2005, Kawachi & Hanawa 1998)

Simple equation of state (EOS)

$$T = \begin{cases} 4.4\rho_{18}^{-0.27} & \rho_{18} < 1 \\ 4.4\rho_{18}^{0.07} & \rho_{18} \geq 1 \end{cases}$$

$\rho_{18} = \rho/(10^{-18}\mathrm{g\,cm^{-3}})$

At $\rho_{18} = 1$ the Bonnor-Ebert mass is $M_{BE} = 0.067\ \mathrm{M}_\odot$ (close to the observed peak of $M = 0.2\ \mathrm{M}_\odot$.

Problem:

- Doesn't explain SF in high density SF regions like Orion Bar.
- EOS does not account for heating by massive stars

RADIATIVE MODELS

Radiative feedback shuts off fragmentation at a characteristic mass scale that sets the peak of the IMF

Assumptions:

We form a small proto-star that radiates at a rate L.

The gas at a distance R then has a temperature

$$L \approx 4\pi R^2 \sigma T^4$$

The Bonnor-Ebert mass as a function of T

$$M_{BE} \approx \frac{c_s^3}{\sqrt{G^3\rho}} = \sqrt{\left(\frac{k_B T}{\mu m_H G}\right)^3 \frac{1}{\rho}}$$

M_{BE} depends on R. At small R, T is large and M_{BE} is also large. At large R, T drops and M_{BE} drops as well.

Compare M_{BE} with the mass enclosed in the radius R

$$M \approx \left(\frac{1}{36\mu}\right)^{\frac{1}{10}} \left(\frac{k_B}{G\mu m_H}\right)^{\frac{6}{5}} \left(\frac{L}{\sigma}\right)^{\frac{3}{10}} \rho^{-\frac{1}{5}}$$

L at this stage is dominated by the accretion

$$L \approx \psi \dot{M}$$

$\psi \approx 10^{14} \mathrm{erg\,g^{-1}}$, and

$$\dot{M} \approx M\sqrt{G\rho}$$

Then

$$M \approx \left(\frac{1}{36\mu}\right)^{\frac{1}{7}} \left(\frac{k_B}{G\mu m_H}\right)^{\frac{12}{7}} \left(\frac{\psi}{\sigma}\right)^{\frac{3}{7}} \rho^{-\frac{1}{14}}$$
$$= 0.3 \left(\frac{n}{100\ \mathrm{cm^{-3}}}\right)^{-1/14} \mathrm{M_\odot}$$

with $n = \rho/(\mu m_H)$

Good match with observations. Simulations seem to confirm that radiative feedback can pick out a characteristic IMF peak mass.